arXiv:hep-ex/0607025v2 18 Aug 2006

Measurements of $\chi_{cJ} \to K^+K^-K^+K^-$ decays

M. Ablikim[1], J. Z. Bai[1], Y. Ban[12], J. G. Bian[1], X. Cai[1], H. F. Chen[17], H. S. Chen[1], H. X. Chen[1], J. C. Chen[1], Jin Chen[1], Y. B. Chen[1], S. P. Chi[2], Y. P. Chu[1], X. Z. Cui[1], Y. S. Dai[20], L. Y. Diao[9], Z. Y. Deng[1], Q. F. Dong[15], S. X. Du[1], J. Fang[1], S. S. Fang[2], C. D. Fu[1], C. S. Gao[1], Y. N. Gao[15], S. D. Gu[1], Y. T. Gu[4], Y. N. Guo[1], Y. Q. Guo[1], Z. J. Guo[17], F. A. Harris[17], K. L. He[1], M. He[13], Y. K. Heng[1], H. M. Hu[1], T. Hu[1], G. S. Huang[1a], X. T. Huang[13], X. B. Ji[1], X. S. Jiang[1], X. Y. Jiang[5], J. B. Jiao[13], D. P. Jin[1], S. Jin[1], Yi Jin[8], Y. F. Lai[1], G. Li[2], H. B. Li[1], H. H. Li[1], J. Li[1], R. Y. Li[1], S. M. Li[1], W. D. Li[1], W. G. Li[1], X. L. Li[1], X. N. Li[1], X. Q. Li[11], Y. L. Li[4], Y. F. Liang[14], H. B. Liao[1], B. J. Liu[1], C. X. Liu[1], F. Liu[6], Fang Liu[1], H. H. Liu[1], H. M. Liu[1], J. Liu[12], J. B. Liu[1], J. P. Liu[19], Q. Liu[1], R. G. Liu[1], Z. A. Liu[1], Y. C. Lou[5], F. Lu[1], G. R. Lu[5], J. G. Lu[1], C. L. Luo[10], F. C. Ma[9], H. L. Ma[1], L. L. Ma[1], Q. M. Ma[1], X. B. Ma[5], Z. P. Mao[1], X. H. Mo[1], J. Nie[1], S. L. Olsen[17], H. P. Peng[17d], R. G. Ping[1], N. D. Qi[1], H. Qin[1], J. F. Qiu[1], Z. Y. Ren[1], G. Rong[1], L. Y. Shan[1], L. Shang[1], C. P. Shen[1], D. L. Shen[1], X. Y. Shen[1], H. Y. Sheng[1], H. S. Sun[1], J. F. Sun[1], S. S. Sun[1], Y. Z. Sun[1], Z. J. Sun[1], Z. Q. Tan[4], X. Tang[1], G. L. Tong[1], G. S. Varner[17], D. Y. Wang[1], L. Wang[1], L. L. Wang[1], L. S. Wang[1], M. Wang[1], P. Wang[1], P. L. Wang[1], W. F. Wang[1b], Y. F. Wang[1], Z. Wang[1], Z. Y. Wang[1], Zhe Wang[1], Zheng Wang[2], C. L. Wei[1], D. H. Wei[1], U. Wiedner[16], N. Wu[1], X. M. Xia[1], X. X. Xie[1], G. F. Xu[1], X. P. Xu[6], Y. Xu[11], M. L. Yan[18], H. X. Yang[1], Y. X. Yang[3], M. H. Ye[2], Y. X. Ye[18], Z. Y. Yi[1], G. W. Yu[1], C. Z. Yuan[1], J. M. Yuan[1], Y. Yuan[1], S. L. Zang[1], Y. Zeng[7], Yu Zeng[1], B. X. Zhang[1], B. Y. Zhang[1], C. C. Zhang[1], D. H. Zhang[1], H. Q. Zhang[1], H. Y. Zhang[1], J. W. Zhang[1], J. Y. Zhang[1], S. H. Zhang[1], X. M. Zhang[1], X. Y. Zhang[13], Yiyun Zhang[14], Z. P. Zhang[18], D. X. Zhao[1], J. W. Zhao[1], M. G. Zhao[1], P. P. Zhao[1], W. R. Zhao[1], Z. G. Zhao[1c], H. Q. Zheng[12], J. P. Zheng[1], Z. P. Zheng[1], L. Zhou[1], N. F. Zhou[1c], K. J. Zhu[1], Q. M. Zhu[1], Y. C. Zhu[1], Y. S. Zhu[1], Yingchun Zhu[1d], Z. A. Zhu[1], B. A. Zhuang[1], X. A. Zhuang[1], B. S. Zou[1]

(BES Collaboration)

[1] *Institute of High Energy Physics, Beijing 100049, People's Republic of China*
[2] *China Center for Advanced Science and Technology (CCAST), Beijing 100080, People's Republic of China*
[3] *Guangxi Normal University, Guilin 541004, People's Republic of China*
[4] *Guangxi University, Nanning 530004, People's Republic of China*
[5] *Henan Normal University, Xinxiang 453002, People's Republic of China*
[6] *Huazhong Normal University, Wuhan 430079, People's Republic of China*
[7] *Hunan University, Changsha 410082, People's Republic of China*
[8] *Jinan University, Jinan 250022, People's Republic of China*
[9] *Liaoning University, Shenyang 110036, People's Republic of China*
[10] *Nanjing Normal University, Nanjing 210097, People's Republic of China*
[11] *Nankai University, Tianjin 300071, People's Republic of China*
[12] *Peking University, Beijing 100871, People's Republic of China*
[13] *Shandong University, Jinan 250100, People's Republic of China*
[14] *Sichuan University, Chengdu 610064, People's Republic of China*
[15] *Tsinghua University, Beijing 100084, People's Republic of China*
[16] *Uppsala University,Department of Nuclear and Particle Physics,Box 535,SE-75121 Uppsala,Sweden.*
[17] *University of Hawaii, Honolulu, HI 96822, USA*
[18] *University of Science and Technology of China, Hefei 230026, People's Republic of China*
[19] *Wuhan University, Wuhan 430072, People's Republic of China*
[20] *Zhejiang University, Hangzhou 310028, People's Republic of China*

[a] *Current address: Purdue University, West Lafayette, IN 47907, USA*
[b] *Current address: Laboratoire de l'Accélérateur Linéaire, Orsay, F-91898, France*
[c] *Current address: University of Michigan, Ann Arbor, MI 48109, USA*
[d] *Current address: DESY, D-22607, Hamburg, Germany*

Using 14M $\psi(2S)$ events taken with the BES-II detector, $\chi_{cJ} \to 2(K^+K^-)$ decays are studied. For the four-kaon final state, the branching fractions are $\mathcal{B}(\chi_{c0,1,2} \to 2(K^+K^-)) = (3.48 \pm 0.23 \pm 0.47) \times 10^{-3}$, $(0.70 \pm 0.13 \pm 0.10) \times 10^{-3}$, and $(2.17 \pm 0.20 \pm 0.31) \times 10^{-3}$. For the ϕK^+K^- final state, the branching fractions, which are measured for the first time, are $\mathcal{B}(\chi \to \phi K^+K^-) = (1.03 \pm 0.22 \pm 0.15) \times 10^{-3}$, $(0.46 \pm 0.16 \pm 0.06) \times 10^{-3}$,

1. Introduction

Exclusive quarkonium decays provide an important laboratory for investigating perturbative quantum chromodynamics. Compared with J/ψ and $\psi(2S)$ decays, there is much less knowledge on χ_{cJ} decays which have parity and charge conjugation $PC = ++$. Relatively few exclusive decays of the χ_{cJ} have been measured. For the $\chi_{cJ} \rightarrow$ Vector Vector (VV) mode, measurements of $\chi_{cJ} \rightarrow \phi\phi$ [1], $K^*(892)^0\bar{K}^*(892)^0$ [2], and $\omega\omega$ [3] have been recently reported. The search for new decay modes and measurements with higher precision will help in better understanding various χ_{cJ} decay mechanisms [4,5] and the nature of ${}^3P_J$ $c\bar{c}$ bound states.

Furthermore, the decays of χ_{cJ}, especially χ_{c0} and χ_{c2}, provide a direct window on glueball dynamics in the 0^{++} and 2^{++} channels since the hadronic decays may proceed via $c\bar{c} \rightarrow gg \rightarrow q\bar{q}q\bar{q}$. Recently, a paper by Zhao [6] points out that the decay branching fractions for scalar glueball candidates ($f_0(1370)$, $f_0(1500)$, and $f_0(1710)$) in χ_{c0} decays may be predicted by a factorization scheme, in which some parameters can be fitted with $\mathcal{B}(\chi_{cJ} \rightarrow \omega\omega, K^*(892)^0\bar{K}^*(892)^0, \phi\phi)$ [6]. The measurement precision of $\mathcal{B}(\chi_{cJ} \rightarrow VV)$ will affect the uncertainties of the fitted parameters. Also, these fitted parameters will help clarify the role played by OZI-rule violation and SU(3) flavor breaking in the decays.

In this analysis, $\chi_{cJ} \rightarrow K^+K^-K^+K^-$ is studied using $\psi(2S)$ radiative decays. The branching fractions of $\chi_{cJ} \rightarrow K^+K^-K^+K^-$ and $\chi_{c0,2} \rightarrow \phi\phi$ are measured with higher statistics, and those of χ_{cJ} decaying to ϕK^+K^- are measured for the first time.

2. The BES detector

The Beijing Spectrometer (BES) is a conventional solenoidal magnet detector that is described in detail in Ref. [7]; BESII is the upgraded version of the BES detector [8]. A 12-layer vertex chamber (VC) surrounding the beam pipe provides trigger and position information. A forty-layer main drift chamber (MDC), located radially outside the VC, provides trajectory and energy loss (dE/dx) information for charged tracks over 85% of the total solid angle. The momenta resolution is $\sigma_p/p = 0.017\sqrt{1+p^2}$ (p in GeV/c), and the dE/dx resolution for hadron tracks is $\sim 8\%$. An array of 48 scintillation counters surrounding the MDC measures the time-of-flight (TOF) of charged tracks with a resolution of $\sim$ 200 ps for hadrons. Outside of the TOF counters is a 12-radiation-length barrel shower counter (BSC) composed of gas tubes interleaved with lead sheets. This measures the energies of electrons and photons over $\sim 80\%$ of the total solid angle with an energy resolution of $\sigma_E/E = 22\%/\sqrt{E}$ (E in GeV). Outside of the solenoidal coil, which provides a 0.4 Tesla magnetic field over the tracking volume, is an iron flux return that is instrumented with three double layers of counters that identify muons of momenta greater than 0.5 GeV/c.

A GEANT3 based Monte Carlo (MC) program with detailed consideration of the detector performance (such as dead electronic channels) is used to simulate the BESII detector. The consistency between data and Monte Carlo has been carefully checked in many high purity physics channels, and the agreement is quite reasonable [9].

3. Event selection

The data sample used for this analysis consists of $(14.00 \pm 0.56) \times 10^6$ $\psi(2S)$ events [10] collected with the BESII detector at the center-of-mass energy $\sqrt{s} = M_{\psi(2S)}$. The $\chi_{cJ} \rightarrow K^+K^-K^+K^-$ channels are investigated using $\psi(2S)$ radiative decays to χ_{cJ}. Events with four charged tracks and one to three photons are selected. Each charged track is required to be well fitted by a helix and to have a polar angle, θ, within the fiducial region $|\cos\theta| < 0.8$. To ensure tracks originate from the interaction region, we require $V_{xy} = \sqrt{V_x^2 + V_y^2} < 2$ cm and $|V_z| < 20$ cm, where V_x, V_y, and V_z are the x, y, and z coordinates of the point of closest approach of each charged track to the beam axis. All charged tracks must be identified as kaons using the combined dE/dx and TOF information.

A neutral cluster is considered to be a photon

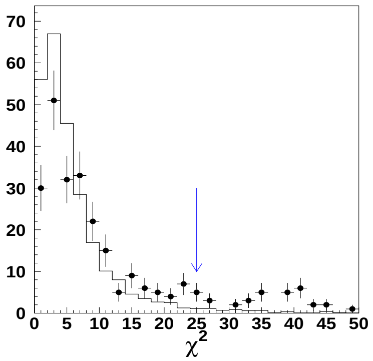

Figure 1. χ^2 distribution of 4-C fit for $\chi_{c0} \to K^+K^-K^+K^-$. Histogram denotes MC and error bars denote data.

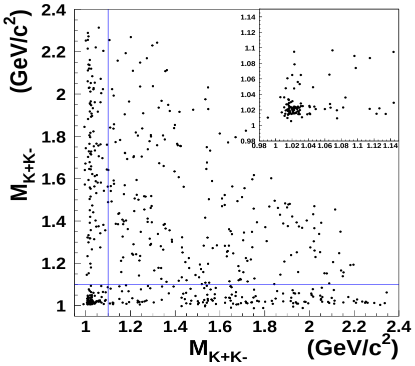

Figure 2. $M^{(1)}_{K^+K^-}$ versus $M^{(2)}_{K^+K^-}$ for candidate events.

candidate if it is located within the BSC fiducial region ($|\cos\theta| < 0.75$), the energy deposited in the BSC is greater than 50 MeV, the first hit appears in the first 6 radiation lengths, the angle between the cluster and the nearest charged track is more than 15°, and the angle between the direction of cluster development and the direction of the photon emission is less than 40°.

A four constraint (4-C) kinematic fit under the $\psi(2S) \to \gamma K^+K^-K^+K^-$ hypothesis is performed, and the χ^2 of the fit is required to be less than 25. For events with two or three photon candidates, the combination having the minimum χ^2 is chosen. In addition, $\chi^2_{\gamma K^+K^-K^+K^-} < \chi^2_{\gamma\pi^+\pi^-\pi^+\pi^-}$ and $\chi^2_{\gamma K^+K^-K^+K^-} < \chi^2_{\gamma\pi^+\pi^-K^+K^-}$ are required to suppress background contamination from $\psi(2S) \to \gamma\pi^+\pi^-\pi^+\pi^-$ and $\psi(2S) \to \gamma\pi^+\pi^-K^+K^-$. Figure 1 shows the χ^2 distribution of data and MC for the process of $\chi_{c0} \to K^+K^-K^+K^-$.

With four selected kaons, there are four ways to combine oppositely charged kaons, and two combinations of $M^{(1)}_{K^+K^-}$ $M^{(2)}_{K^+K^-}$ pairs can be formed. The combination that has one of its $M_{K^+K^-}$ closest to the ϕ mass is selected for further analysis.

Figure 2 shows the distribution of $M_{K^+K^-}$ versus $M_{K^+K^-}$ for selected events. There are two clear bands near 1.02 GeV/c^2 which correspond to the ϕK^+K^- final state. The insert in the upper right corner, is the enlarged view of the lower left corner, and a clear $\phi\phi$ signal can be seen. Figure 3 shows the corresponding $M^{(1)}_{K^+K^-}$ versus $M^{(2)}_{K^+K^-}$ distribution for MC $\psi(2S) \to \gamma\chi_{c1}$, $\chi_{c1} \to \phi K^+K^-$ and $\phi\phi$, using $\mathcal{B}(\chi_{c1} \to \phi K^+K^-) : \mathcal{B}(\chi_{c1} \to \phi\phi)$=2:1.

To investigate intermediate resonances in (K^+K^-) final states, the invariant mass distribution of all four possible K^+K^- combinations are plotted in Figure 4(a). Except for the ϕ, no other obvious resonance is seen.

To test if the above selection criteria will cause "fake" ϕ signals, $\psi(2S) \to \gamma\chi_{c1}, \chi_{c1} \to K^+K^-K^+K^-$ MC events are generated according to phase space. Figure 4(b) shows the $M_{K^+K^-}$ distribution of these events using the same selection as for data. No peak is seen around the ϕ signal region.

4. MC simulation

For each of the channels studied 100,000 MC events are generated. The proper angular distributions for the photons emitted in $\psi(2S) \to \gamma\chi_{cJ}$ are used [11]. Phase space is used for the $\chi_{cJ} \to$

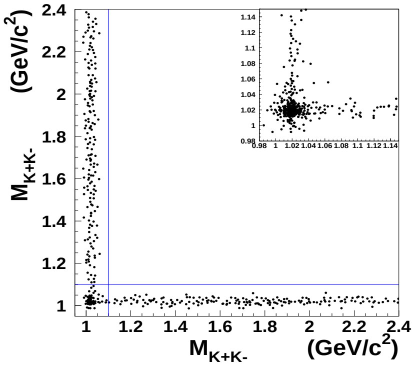

Figure 3. $M^{(1)}_{K^+K^-}$ versus $M^{(2)}_{K^+K^-}$ for MC $\psi(2S) \to \gamma\chi_{c1}$, $\chi_{c1} \to \phi K^+K^-$ and $\phi\phi$ events after event selection.

$2(K^+K^-)$ decays (including intermediate states, e.g. $\chi_{cJ} \to \phi\phi$).

5. Background study

Possible backgrounds come from $\psi(2S) \to \gamma\chi_{cJ}$, $\chi_{cJ} \to \pi^+\pi^-\pi^+\pi^-$, $\pi^+\pi^-K^+K^-$, $K_sK\pi$, and $\pi^+\pi^-p\bar{p}$; $\psi(2S) \to \pi^0K^+K^-K^+K^-$; and phase space $\psi(2S) \to \gamma K^+K^-K^+K^-$. 100,000 MC events are generated for each of the first four background channels where the angular distribution for the radiative photon is generated the same as for the signal channels while the χ_{cJ} decays are generated according to phase space. The contamination from these backgrounds to each signal channel is less than 1.0%, which is negligible. 100,000 MC events are also generated for each of the last two background channels according to phase space. For $\psi(2S) \to \pi^0K^+K^-K^+K^-$, Figure 5(a) shows the $M_{K^+K^-K^+K^-}$ distribution in the region 3.2-3.7 GeV/c^2. Using the branching fraction measured by CLEOc [12], the number of events from this channel is expected to be 23 ± 7. For $\psi(2S) \to \gamma K^+K^-K^+K^-$, the $M_{K^+K^-K^+K^-}$ distribution is shown in Figure 5(b). This branching fraction is currently unavailable. However, comparing the $M_{K^+K^-K^+K^-}$ distribution from this channel and that from data, shown in Figure 6, the contribution from $\psi(2S) \to \gamma K^+K^-K^+K^-$ background should be small. No χ_{cJ} peaks are seen in Figure 5(a) and (b). Thus, the fitted number of χ_{cJ} signal events is insensitive to the shape of the function used to describe the total background.

We have also considered possible background from $\psi(2S) \to \gamma\chi_{c0}, \chi_{c0} \to f_0(980)f_0(980) \to K^+K^-K^+K^-$. Using the branching ratio for $\chi_{c0} \to f_0(980)f_0(980) \to \pi^+\pi^-K^+K^-$ [13], the ratio $B(f_0(980) \to K^+K^-)/(B(f_0(980) \to K^+K^-) + B(f_0(980) \to \pi^+\pi^-))$ [13], and MC efficiencies for these processes, the estimated number of $f_0(980)f_0(980) \to K^+K^-K^+K^-$ events is about 6, which are spread over a relatively wide region compared with the width of the ϕ [14]. Thus, this background in the ϕ region is negligibly small.

6. Mass spectrum fit

6.1. $\chi_{cJ} \to 2(K^+K^-)$

Figure 6(a) shows the high mass ($>$ 3.2 GeV/c^2) $2(K^+K^-)$ invariant mass distribution using all candidate events in $\psi(2S) \to \gamma\chi_{cJ}, \chi_{cJ} \to 2(K^+K^-)$. Clear χ_{cJ} signals can be seen in this Figure. A fit with Breit-Wigner functions convoluted with Gaussian resolution functions (about 15 MeV/c^2 for χ_{cJ} signals in all channels studied) yields the number of χ_{cJ} events: $N_{\chi_{c0}} = 278 \pm 18$, $N_{\chi_{c1}} = 54 \pm 10$, and $N_{\chi_{c2}} = 160 \pm 14$. MC simulation gives detection efficiencies of 5.9%, 6.3%, and 5.8% for $J = 0$, 1, and 2, respectively.

6.2. $\chi_{cJ} \to \phi K^+K^-$

The $\chi_{cJ} \to \phi K^+K^-$ events are clustered as two bands around the ϕ mass in Figure 2. The ϕK^+K^- region is defined by $M^{(i)}_{K^+K^-} \in (1.08, 2.4)$ GeV/c^2 and $M^{(j\neq i)}_{K^+K^-} \in (1.00, 1.04)$ GeV/c^2 (i, j = 1, 2). Figure 6(b) shows the $M_{\phi K^+K^-}$ distribution for these events, and clear χ_{cJ} signals can be seen. MC simulation gives detection efficiencies of 5.9%, 6.2%, and 5.6% for J=0, 1, and 2, respectively. A fit with Breit-Wigner functions convoluted with Gaussian resolution functions yields the number of χ_{cJ} events:

$N_{\chi_{c0}} = 53.5 \pm 8.3$, $N_{\chi_{c1}} = 19.2 \pm 5.6$, and $N_{\chi_{c2}} = 56.3 \pm 8.2$.

In order to determine the contribution from non-resonant $\psi(2S) \to \gamma\chi_{cJ}, \chi_{cJ} \to 2(K^+K^-)$ events in the ϕK^+K^- region, we analyze the non-resonant $2(K^+K^-)$ region, defined by $M^{(i)}_{K^+K^-} \in (1.1, 2.4)$ GeV/c^2 (i = 1,2) in Figure 2. The number of events in this region is $N^{nr}_t = 238$. Figure 7(a) shows the $M_{K^+K^-K^+K^-}$ distribution for the non-resonant $2(K^+K^-)$ region events, where three clean χ_{cJ} peaks are seen with very little background. A fit with Breit-Wigner functions convoluted with Gaussian resolution functions yields: $N_{\chi^{nr}_{c0}} = 144.1 \pm 12.7$, $N_{\chi^{nr}_{c1}} = 21.5 \pm 5.5$, and $N_{\chi^{nr}_{c2}} = 39.4 \pm 6.9$.

Figure 7(b) shows the ϕ signal for the ϕK^+K^- region events. The fit yields 143 ± 14 signal events and $N_{bg} = 25$ background events from non-resonant $2(K^+K^-)$ events within a 3σ window (1.00 - 1.04 GeV/c^2) in the ϕ signal region. We calculate the non-resonant $2(K^+K^-)$ contribution to $N_{\chi_{c0}}$, $N_{\chi_{c1}}$, and $N_{\chi_{c2}}$ assuming that the proportion of χ_{c0}, χ_{c1}, and χ_{c2} events is the same for non-resonant $2(K^+K^-)$ events in the non-resonant and the ϕK^+K^- regions. For χ_{c0}, the non-resonant contribution is $N^n_{\chi_{c0}} = N^{nr}_{\chi_{c0}} \cdot N_{bg}/N^{nr}_t = 15.1 \pm 1.3$. Similarly, we obtain $N^n_{\chi_{c1}} = 2.3 \pm 0.6$, and $N^n_{\chi_{c2}} = 4.1 \pm 0.7$. Therefore, the number of ϕK^+K^- events, after subtracting the non-resonant $2(K^+K^-)$ events, is $N_{\chi_{c0}} = 38.4 \pm 8.4$, $N_{\chi_{c1}} = 16.9 \pm 5.6$, and $N_{\chi_{c2}} = 52.2 \pm 8.2$.

6.3. $\chi_{cJ} \to \phi\phi$

The signal region for $\chi_{cJ} \to \phi\phi$ events is a 40 MeV/c^2× 40 MeV/c^2 square around the ϕ mass in Figure 2. Figure 8 shows the $M_{\phi\phi}$ distribution for these $\phi\phi$ events, and clear $\chi_{c0,2}$ signals can be seen. MC simulation gives detection efficiencies of 9.0% and 8.6% for J=0 and 2, respectively. A fit yields the number of events for χ_{cJ}: $N_{\chi_{c0}} = 27.8 \pm 5.8$ and $N_{\chi_{c2}} = 42.7 \pm 7.1$.

The two bands near the ϕ mass in Figure 2, used to extract the $\chi_{cJ} \to \phi K^+K^-$ signal in Section 6.2, are taken as the sideband region for the $\phi\phi$ events. They include both the ϕK^+K^- events and non-resonant $K^+K^-K^+K^-$ events. From MC simulation the event distributions in the two bands are nearly uniform. The number of normalized sideband events in the $\phi\phi$ signal region are

$$N^{sd}_{\chi_{c0}} = \frac{53.5 \pm 8.3}{f} \approx 1.6 \pm 0.3,$$

$$N^{sd}_{\chi_{c2}} = \frac{56.3 \pm 8.2}{f} \approx 1.7 \pm 0.3,$$

respectively, where the factor f=33 is the ratio of the sideband area to the $\phi\phi$ signal region area. Thus we obtain the number of events in $\chi_{cJ} \to \phi\phi$: $N_{\chi_{c0}} = 26.2 \pm 5.8$ and $N_{\chi_{c2}} = 41.0 \pm 7.1$.

7. Systematic error

The systematic error in these branching fraction measurements includes the uncertainties caused by wire resolution, particle ID, photon efficiency, and the number of $\psi(2S)$ events.

The systematic error caused by MDC tracking and the kinematic fit are estimated by using simulations with different MDC wire resolutions [9]. For particle ID, the combined information of dE/dx and TOF is used. An error of 2% is assigned for each charged track [16] and each photon [9]. The errors introduced by branching fractions of intermediate states are taken from the Particle Data Group (PDG) [15].

The total systematic errors, determined by the sum of all sources added in quadrature, are listed in Table 1. The uncertainty from $\mathcal{B}(\phi \to K^+K^-)$ contributes once in the systematic error estimation for $\chi_{cJ} \to \phi K^+K^-$ and twice in $\phi\phi$, while it does not contribute in $\chi_{cJ} \to 2(K^+K^-)$. For the uncertainties caused by wire resolution, there are some slight differences for the different decay channels.

8. Results

For $\chi_{cJ} \to 2(K^+K^-)$ (including intermediate states), the branching fractions are calculated using

$$\mathcal{B}(\chi_{cJ} \to 2(K^+K^-)) = \frac{N_{\chi_{cJ}}}{N_{\psi(2S)} \cdot \mathcal{B}(\psi(2S) \to \gamma\chi_{cJ}) \cdot \bar{\epsilon}},$$

Table 1
Systematic error (%). In the wire resolution row, the numbers from left to right correspond to $\psi(2S) \to 2(K^+K^-)$, ϕK^+K^-, and $\phi\phi$.

Source		χ_{c0}	χ_{c1}	χ_{c2}
Wire resolution		8.9, 9.8, 10.0	9.3, 9.9	9.7, 9.6, 10.1
Particle ID		8	8	8
Photon efficiency		2	2	2
Background shape		negligible	negligible	negligible
Number of $\psi(2S)$		4	4	4
$\mathcal{B}(\psi(2S) \to \gamma\chi_{cJ})$		4.3	4.6	4.9
$\mathcal{B}(\phi \to K^+K^-)$		1.2	1.2	1.2
Total	$\chi_{cJ} \to 2(K^+K^-)$	13.5	13.9	14.3
	$\chi_{cJ} \to \phi K^+K^-$	14.1	14.3	14.2
	$\chi_{cJ} \to \phi\phi$	14.3	-	14.5

where, the average detection efficiency $\bar{\epsilon}$ is given by

$$\bar{\epsilon} = \frac{N_{\chi_{cJ}} - N_{\phi K^+K^-} - N_{\phi\phi}}{N_{\chi_{cJ}}} \cdot \epsilon_{2(K^+K^-)} + \frac{N_{\phi K^+K^-}}{N_{\chi_{cJ}}} \cdot \epsilon_{\phi K^+K^-} + \frac{N_{\phi\phi}}{N_{\chi_{cJ}}} \cdot \epsilon_{\phi\phi}.$$

Similarly, we can calculate the branching fractions for $\chi_{cJ} \to \phi K^+K^-$, $\phi\phi$ with corresponding efficiency expressions. Table 2 lists our measurement results, together with the PDG values.

In summary, the decays of $\chi_{cJ} \to 2(K^+K^-)$ are studied, and the corresponding branching fractions including intermediate states are given. The decay $\chi_{cJ} \to \phi K^+K^-$ is observed for the first time. The branching fractions for $\chi_{cJ} \to 2(K^+K^-)$ and $\chi_{cJ} \to \phi\phi$ are measured with higher precision; Table 2 lists the comparison of the measured branching fractions between BESII and the PDG. Our measurement for $\chi_{cJ} \to \phi\phi$, together with the two measurements of $\chi_{cJ} \to \omega\omega$ and $\bar{K}^*(892)^0 K^*(892)^0$, will be helpful in understanding the nature of χ_{cJ} states.

9. Acknowledgments

The BES collaboration thanks the staff of BEPC and computing center for their hard efforts. This work is supported in part by the National Natural Science Foundation of China under contracts Nos. 10491300, 10225524, 10225525, 10425523, the Chinese Academy of Sciences under contract No. KJ 95T-03, the 100 Talents Program of CAS under Contract Nos. U-11, U-24, U-25, and the Knowledge Innovation Project of CAS under Contract Nos. U-602, U-34 (IHEP), the National Natural Science Foundation of China under Contract No. 10225522 (Tsinghua University), the Swedish research Council (VR), and the Department of Energy under Contract No.DE-FG02-04ER41291 (U Hawaii).

REFERENCES

1. BES Collaboration, J. Z. Bai *et al.*, Phys. Rev. D 60 (1999) 072001.
2. BES Collaboration, M. Ablikim *et al.*, Phys. Rev. D 70 (2004) 092003.
3. BES Collaboration, M. Ablikim *et al.*, Phys. Lett. B 630 (2005) 7.
4. C. Amsler and F. Close, Phys. Rev. D 53 (1996) 295.
5. H. Q. Zhou, R. G. Ping, B. S. Zou, Phys. Lett. B 611 (2005) 123.
6. Qiang Zhao, Phys. Rev. D 72 (2005) 074001.
7. BES Collaboration, J. Z. Bai *et al.*, Nucl. Instr. Meth. A 344 (1994) 319.
8. BES Collaboration, J. Z. Bai *et al.*, Nucl. Instr. Meth. A 458 (2001) 427.
9. BES Collaboration, M. Ablikim *et al.*, Instr. Meth. A 552 (2005) 344.

Table 2
$\chi_{cJ} \to 2(K^+K^-)$ branching fractions.

Channel	$2(K^+K^-)(\times 10^{-3})$		$\phi K^+K^-(\times 10^{-3})$	$\phi\phi(\times 10^{-3})$	
	BES-II	PDG	BES-II	BES-II	PDG
χ_{c0}	$3.48 \pm 0.23 \pm 0.47$	2.1 ± 0.4	$1.03 \pm 0.22 \pm 0.15$	$0.94 \pm 0.21 \pm 0.13$	0.9 ± 0.5
χ_{c1}	$0.70 \pm 0.13 \pm 0.10$	0.39 ± 0.17	$0.46 \pm 0.16 \pm 0.06$	$-$	$-$
χ_{c2}	$2.17 \pm 0.20 \pm 0.31$	1.41 ± 0.35	$1.67 \pm 0.26 \pm 0.24$	$1.70 \pm 0.30 \pm 0.25$	1.9 ± 0.7

10. X. H. Mo *et al.*, HEP&NP, 28 (2004) 455.
11. Mark-I Collaboration, W. Tanenbaum *et al.*, Phys. Rev. D 17 (1978) 1731; G. Karl, S. Meshkov, and J. L. Rosner, *ibid* 13 (1976) 1203; Crystall Ball Collaboration, M. Oreglia *et al.*, *ibid* 25 (1982) 2259.
12. CLEOc collaboration, R. A. Briere,*et al*, Phys. Rev. Lett. 95 (2005) 062001.
13. BES Collaboration, M. Ablikim *et al.*, Phys. Rev. D 72 (2005) 092002.
14. BES Collaboration, M. Ablikim *et al.*, Phys. Lett. B 607 (2005) 243.
15. Particle Physics Group, W. _M. Yao *et al.*, J. Phys. G: Nucl. Part. Phys. 33. 1 (2006) 920.
16. BES Collaboration, M. Ablikim *et al.*, Phys. Lett. B 614 (2005) 37.

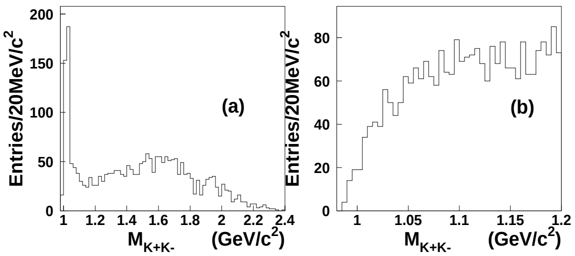

Figure 4. $M_{K^+K^-}$ distribution of all four possible K^+K^- combinations. (b) $M_{K^+K^-}$ distribution for MC $\psi(2S) \to \gamma\chi_{c1}, \chi_{c1} \to K^+K^-K^+K^-$.

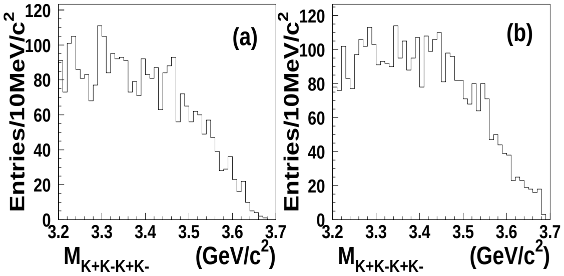

Figure 5. Background shape obtained from MC simulation. (a) $\psi(2S) \to \pi^0 K^+K^-K^+K^-$. (b) $\psi(2S) \to \gamma K^+K^-K^+K^-$.

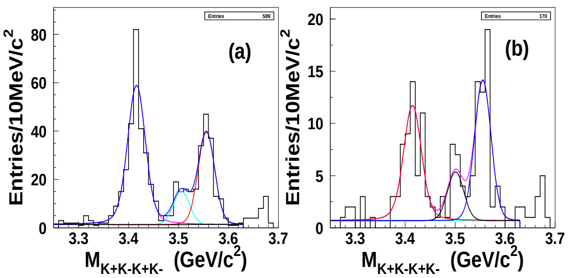

Figure 6. Breit-Wigner fit to χ_{cJ} signals (a) with all candidate events and (b) with the ϕK^+K^- region events.

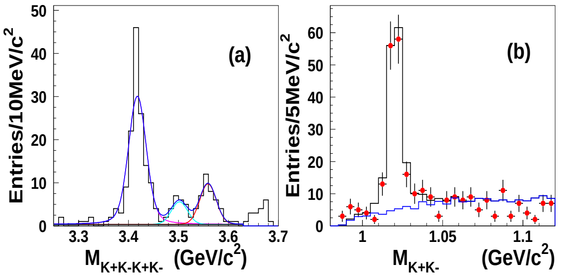

Figure 7. (a) Breit-Wigner fit to χ_{cJ} using non-resonant $2(K^+K^-)$ region events. (b) Fit to ϕ signal with ϕK^+K^- region events.

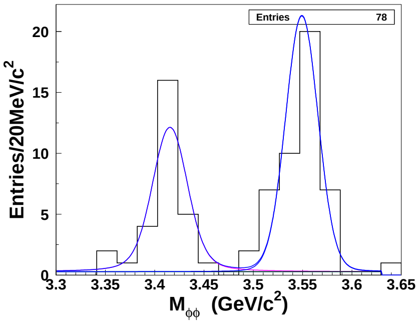

Figure 8. Fit to χ_{cJ} signals in $\phi\phi$ final state.